LA-UR-79-1987

CONF-790913--2

MASTER

TITLE: INTERWELL TRACER ANALYSES OF A HYDRAULICALLY FRACTURED GRANITIC GEOTHERMAL RESERVOIR

(SPE Paper No. 8270)

AUTHOR(S): Jefferson W. Tester, Robert M. Potter, and Robert L. Bivins

SUBMITTED TO: 54th Annual Technical Conference and Exhibition of the Society of Petroleum Engineers of AIME
Las Vegas, Nevada
September 23-26, 1979

University of California

LOS ALAMOS SCIENTIFIC LABORATORY
Post Office Box 1663 Los Alamos, New Mexico 87545
An Affirmative Action/Equal Opportunity Employer

Form No. 836 R3
St. No. 2629
12/78

UNITED STATES
DEPARTMENT OF ENERGY
CONTRACT W-7405-ENG. 36

SPE
Society of Petroleum Engineers of AIME

ABSTRACT

Field experiments using fluorescent dye and radioactive tracers (Br^{82} and I^{131}) have been employed to characterize a hot, low-matrix permeability, hydraulically-fractured granitic reservoir at depths of 2440 to 2960 m (8000 to 9700 ft). Tracer profiles and residence time distributions have been used to delineate changes in the fracture system, particularly in diagnosing pathological flow patterns and in identifying *new injection and production zones. The effectiveness* of one- and two-dimensional theoretical dispersion models utilizing single and multiple porous, fractured zones with velocity and formation dependent effects are discussed with respect to actual field data.

INTRODUCTION

The geometry of the boreholes, fractures, and injection and production zones are described in previous reports and papers[1,2,3]. Field tests of a prototype, two wellbore, hot dry rock geothermal reservoir are being conducted by the Los Alamos Scientific Laboratory at the Fenton Hill site located near the Valles Caldera in the Jemez Mountains of north central New Mexico. Extensive testing of this hydraulically fractured system in low matrix permeability granite at 150 to 200°C and depths of 2-3 km (6500 to 10,000 ft) has been conducted for the last four years to characterize fracture initiation and propagation, flow distribution and impedance, reservoir size, fluid loss due to permeation, geochemistry and induced seismic effects under heat extraction conditions ranging from <1 to 5 MW(t). The results of several major closed-loop circulation tests are covered in detail by Murphy and Tester[3] and Tester and Albright[4].

This paper focuses on one particular aspect of flow diagnostics, namely the use of tracers to characterize (1) injection and production zone flow paths near the wellbores and (2) fracture volume, residence time distributions and the degree of fluid mixing within the fractured region. In the first case, information from temperature, spinner, caliper and borehole televiewer logs were used in conjunction with I^{131} and Br^{82} tracer logs under fluid injection and production conditions to construct a consistent model of normal and pathological flow regions within the fractured reservoir as well as benind casing and at various borehole-to-fracture connections[1,4,5]. In the second case, because of the relatively small volume of the combined wellbore and fracture system, ~150,000 ℓ (40,000 gal), residence times were short and repeated tests were run. Residence time distributions (RTD) *were determined in response to a tracer pulse injected* into one well (EE-1) and produced in a second well (GT-2) directly connected to the fractured region. Variations in the RTD's illustrate directly the mean size and distribution of flow velocities in the connected system. As Wagner et al[6,7] and Onats[8] point out, these techniques can be very useful to the reservoir engineer in characterizing complex flow systems. For example, experimental RTD's for this reservoir were used to design a formation chemical treatment using sodium carbonate to selectively dissolve the quartz component of the biotite granodiorite reservoir rock at depth[1]. In this case, the *distribution of residence times was superimposed onto an* expression for the dissolution reaction kinetics of quartz to arrive at a predicted concentration breakthrough of reaction products. Other applications to groundwater migration, volumetric sweep efficiencies in flooding, flow short circuiting and other pathological flow problems have received attention in recent years[6-12]. For our particular application to fractured, hot dry rock (HDR) geothermal systems, identification of injection and production zone profiles and casing cement integrity and the relationship between flow distribution and fracture size (area and volume) are important in establishing the thermal capacities and production lifetimes of actual HDR geothermal reservoirs.

In addition to developing field techniques and borehole surveying equipment for high temperature environments[1,2], theoretical models were formulated to characterize fluid dispersion for a variety of assumptions related to specific formation properties and flow geometries. Reservoir heterogenities were

Work conducted under the auspices of the U.S. DOE.
References and illustrations at end of paper.

introduced by using either multiple porous zone regions or by using velocity-dependent, anisotropic dispersion coefficients.

THEORY

Considerable effort has been extended in the past toward developing analytic and numerical approaches to the problem of dispersion in porous media flow[6-22]. In general, the following diffusion-type equation is solved with a variety of boundary and initial conditions:

$$\nabla\cdot(D\nabla C) - \vec{u}\cdot\nabla C = \frac{\partial C}{\partial t} \quad \ldots\ldots (1)$$

where D is the effective dispersion coefficient tensor and can depend on both flow velocity and formation properties. As the degree of mixing increases, the magnitude of D increases. D can be directionally dependent and very complex in mathematical form[20,21]. Furthermore, the introduction of stagnant or dead end pore regions lead to capacitance effects which increase the apparent degree of mixing [17,18,19]. In this paper these effects are neglected. Solutions to Eq. (1) were considered for velocity dependent and independent dispersion coefficients in one and two dimensions.

In the one-dimensional case two models were developed with only formation dependent dispersion coefficients (D^o) used. Equation (1) reduces to:

$$D^o \frac{\partial^2 C}{\partial x^2} + u \frac{\partial C}{\partial x} = \frac{\partial C}{\partial t} \quad \ldots\ldots (2)$$

Solutions given by Brenner[13] were adapted to provide exit tracer concentrations in response to a pulse injection. These are commonly referred to as residence time distributions. C can be represented as either a series solution or in a modified asymtotic equation for large Peclet numbers. Brenner[13] suggests using the asymtotic equation only when Pe>16; however, we found accurate results even with Pe as low as 4,

$$C = C(X,\theta,Pe) \quad \ldots\ldots (3)$$

where $X = x/L$

$$\theta = \frac{ut}{L} = \frac{q}{V}t$$

$$Pe = \frac{uL}{D^o}$$

Adjustments were made to Pe to minimize the following objective function, F, over N data points

$$F = \sum_{i=1}^{N} (C(X_i,\theta_i,Pe) - C_i)^2 \quad \ldots\ldots (4)$$

When F was minimized, an optimum value of Pe resulted.

A multizone model was also developed which assumed independent, one-dimensional dispersion in M separate zones. The predicted tracer concentration response is given by,

$$C = \sum_{j=1}^{M} \xi_j C^j(X_j,\theta_j^*,Pe_j) \quad \ldots\ldots (5)$$

where ξ_j is the flow fraction through zone j and θ_j^* is modified as follows:

$$\theta_j^* = \frac{\xi_j \theta}{\psi_j} \quad \ldots\ldots (6)$$

The same objective function F can then be used to calculate optimal values of Pe_j, ξ_j, and ψ_j. In some cases it may be possible to fix ξ_j or ψ_j resulting in only M adjustable parameters. As M gets large, very complex residence time distributions can be easily matched.

A two-dimensional flow model was also developed and is described in detail in Appendix A. Both velocity and formation dependent dispersion parameters were considered by proposing that D could be expressed as[16]:

$$D_x = \alpha_x u + D^o$$

$$D_y = \alpha_y v + D^o \quad \ldots\ldots (7)$$

D^o accounts for both molecular diffusion, tortuosity and other heterogeneous formation effects. Type curves presented in Appendix A were developed to express exit tracer concentration in the production well in response to a step input in concentration in the injection well for changes in α_x, α_y, and Pe^*. A steady-state velocity profile for two-well potential flow in a homogeneous isotropic porous medium was assumed. The medium could be a large homogeneous zone of height h and infinite radial extent, or a large fracture with aperture h.

EQUIPMENT AND PROCEDURES

Radioactive tracer placement and detection methods for wellbores

The problem of following the flow of fluid into and through complex fracture systems contained between two wellbores has been greatly aided by the use of radioactive tracer techniques developed for oil and gas reservoir analysis. Introduction of the tracer into the flow system was originally done with a conventional injector system - gamma ray detector logging tool. Minimal success with the injector tool, resulting from failure due to high temperatures led to the method of releasing the tracer by explosively breaking a sample container. Measurement of the gamma ray activity was made by means of standard Geiger detectors employing high temperature solid state electronics in the later surveys.

The first four tracer surveys used I^{131}, a separated fission product with a half life of 8 days and a maximum gamma ray energy of 0.36 Mev. Although the results from these experiments were useful, certain inherent disadvantages of the I^{131} isotope became apparent. Its half life of 8 days, though short, leads to a high background if tracer tests are to be scheduled at intervals less than 2 months. Of more concern than this is the high biologic selectivity of the human thyroid gland for iodine and this fact has led to a very low allowable limit of I^{131} concentration in fluids released into surface storage. A further disadvantage was the method of loading the tracer sample into the tool. It resulted in higher radiation doses to the hands of the service personnel than were felt to be necessary. A new tracer dispenser/gamma detector package was designed (Fig. 1) for Br^{82}, an isotope that is easily generated by

neutron activation in a nuclear reactor. Ammonium bromide, encapsulated in a quartz vial, was irradiated in the Los Alamos reactor producing Br^{82} ($t_{1/2}$=36 hrs; maximum gamma ray energy = 1.5 Mev) by neutron capture and then loaded into a heavy metal shielded container in a hot cell. The Br^{82} isotope appears to be almost ideal from the standpoint of half life, biologic sensitivity, gamma ray energy and like iodine, it should have low absorbtivity on the rock surfaces. This container was fitted into a further shielded carrying case for transportation to the site. At the wellhead the logging probe containing the gamma counter was connected to the heavy metal shield containing the capsule. After lowering to the desired depth the capsule was *mechanically broken by a ram. The extension of the ram* also moved a piston causing a flow of trapped water to multiply flush the broken capsule.

Residence time distribution experiments

The dye tracer experiments involved placement of a pulse of concentrated sodium fluorescein dye, typically about 400 liters (100 gal) of 200-300 ppm aqueous solution, into the EE-1 injection wellbore. The pulse was then pumped down through the casing, through the fractured region in the formation, and recovered in the GT-2 production wellbore. The recovered dye concentration was monitored spectrophotometrically at the surface as a function of time and volume throughput. Dye pulses were injected without disruption during fluid circulation through the EE-1/GT-2 system. Because of the relatively short residence times (<10 hr) compared to the overall circulation time (~1800 hr), a fully-developed, steady-state fluid velocity profile was assumed[4]. Extensive testing of the sodium fluorescein-granite-water system showed that neither decomposition nor absorption of dye occurred at any measurable level during 24 hr exposures at 200°C. The detection limit during field experiments was approximately 0.05 ppm or a factor of 4000 to 6000 reduction over the feed composition. Because the openhole and casing string volumes in both EE-1 and GT-2 were well known, borehole volume effects could be eliminated, and fractured reservoir volumes and corresponding residence times could be determined very accurately, to ±800 liters (200 gal).

EXPERIMENTAL RESULTS

The use of the radioactive tracers, I^{131} and Br^{82}

The injection borehole EE-1 was initially fractured below a packer set at 2925 m (9600 ft) and then cased to the packer depth. Cement bond and temperature logs before and after flow tests indicated that the cement behind the casing was slowly failing presumably from extensive thermal cycling. An I^{131} tracer survey was run (3/19/76) to measure both the extent of damage and location of flow sinks. Figure 2 shows a history of a 20 m Ci tracer pulse as it was pumped down the casing and split into two portions. The location of the pulse was followed below the casing to a depth of 2940 m (9645 ft) at which time the gamma detector failed probably because of the high temperature (200°C) encountered. The change in the fluid velocity at ~2940 m (9645 ft) indicated the top of a flow sink, in agreement with temperature surveys. The difference in flow of 1.3 l/s (20 gpm) confirmed the existence of a major flow path behind the casing. Figure 3 contains a series of temperature surveys in EE-1 which show progressive localized cooling of the wellbore. The original hydraulic fracture is shown as anomaly number 1. This location is better defined by the initial tracer survey.

A later temperature log (1-26-77) following further large flow tests indicated the growth of a major flow sink centered at ~2745 m (9000 ft). A second tracer survey was run specifically to define this anomalous region. A 10 m Ci I^{131} tracer pulse was pumped down and then behind the casing at a flow rate of 2.1 l/s (34 gpm). The location of the tracer was followed as it moved up behind the casing. Several sweeps of the logging tool below 2775 m (9105 ft) showed a relatively constant shape and amplitude of the ascending pulse. Figure 4 shows the change in this shape as the tracer pulse reaches a depth of 2767 m (9080 ft). The great majority of the tracer entered a flow sink above this depth. Later venting of the fluid *showed the tracer reappearing at 2758 m (9050 ft).* The zone defined by these two depths agreed almost exactly with that inferred to be a fracture zone from a post-drilling 4-arm caliper log in EE-1. This was the first evidence that natural fractures in our reservoir might be providing openings for a flow *system.*

The third tracer survey followed an attempt to reduce the system impedance by use of sodium carborate as a leaching agent. The temperature survey of 6-16-77 (Fig. 3) following this experiment showed both new flow sinks and further cooling of the original ones. This tracer survey showed the majority of flow leaving at anomaly no. 4 (Fig. 3) but in addition the tracer could be followed in its path to the higher anomalies.

The previous flow tests and accompanying experiments indicated that the communication between the injection borehole EE-1 and the production borehole GT-2 was not adequate to conduct a significant heat extraction experiment. A greatly reduced impedance between the two boreholes was provided by redrilling the lower portion of GT-2. This new system (EE-1/GT-2B) was tested in an 1800 hr (75 day) heat extraction experiment[4]. A fourth tracer survey was run after this operation in order to study both the fracture connections in the two boreholes and the flow paths between them. The tracer was again injected in EE-1 and pumped into the various openings both below and behind the casing. The complex path of the tracer is shown in Fig. 5. This survey shows measurable flow into new openings below the main 2760 m (9055 ft) fracture zone. These sinks may be those shown as anomalies 2 and 3 in Fig. 3. Simultaneous surveying of the gamma activity in GT-2B showed the arrival of the tracer at the multiple production zones. The *sequential appearance of the tracer at the three main* zones suggests that the GT-2B borehole is connected in parallel to a main flow system.

The next tracer test was notable for several reasons. It employed a completely new system using Br^{82} as the tracer instead of I^{131}. In addition, the tracer was released and followed during a period of high flow rate and high back pressure. The results were therefore more useful in interpreting data from the major flow tests than those from earlier tracer tests in which low flow rates were employed. The damage to the cement had increased to such an extent that a significant portion of the flow was exiting through the cement above 2745 m (9000 ft). The movement of the tracer upwards behind the casing allowed an estimate of flow rate and its history. Measurements in GT-2B (Fig. 6) again showed the positions of the main connecting fractures and arrival times for the tracer at each fracture. Contributions from these individual joints connected to GT-2B are obviously present with the observed RTD being a composite of these superimposed flows.

Recementing of the EE-1 casing was then attempted *in order to isolate the fracture system originating at* ~2760 m (9055 ft) and also to seal the leak in the cement. The last test to date, measured the path that fluid now takes in the recemented EE-1 wellbore and subsequently in the GT-2B wellbore. The tracer leaves the EE-1 wellbore entirely below the casing demonstrating the success of the recementing job.

Residence time distribution studies

To evaluate the experimental residence time distributions several simple normalization procedures were used. The results of the four experiments conducted during the 75-day flow test and their statistical analysis are summarized in Table 1 and Figs. 7 and 8. The distributions have been characterized using integral (first moment) mean volumes, median volumes, integral mean volumes using a trimmed section of the distribution, and variances of the normalized distributions. These can be expressed using the following equations and definitions:

$$C_0 = C_i \Big/ \frac{1}{\langle V \rangle} \int_0^\infty C_i dV = \text{normalized concentration}$$

$$\langle V \rangle = \int_0^\infty V C_i dV \Big/ \int_0^\infty C_i dV = \text{integral mean volume}$$

$$[V] = \text{median volume} \int_0^{[V]} C_i dV \Big/ \int_0^\infty C_i dV = 0.5$$

$$|V| = \int_0^{V^*} V C_i dV \Big/ \int_0^{V^*} C_i dV = \text{trimmed mean volume},$$

$\bar{\tau} = \langle V \rangle / \bar{q}$ = integral mean residence time, and

$$\sigma_0^2 = \text{C}_0 \text{ distribution variance} = \int_0^\infty V^2 C_i dV \Big/ \langle V \rangle^2 \int_0^\infty C_i dV - 1 \ .$$

Flow in the fracture system can be described as well-mixed with no major short circuits. Dispersion of fluid in a single, propped hydraulic fracture cannot account for all of the mixing. Because of this and the *known existence of multiple flow paths between EE-1 and* GT-2B[3,4], the observed shape of the RTD is caused by dispersion within individual flow paths as well as superposition from mixing of various production flows in the wellbore. Consequently, several statistical quantities are needed to describe flow in the system. The median volume probably adequately represents the *flow through the major production paths in GT-2B, while* the increase in the spread of the distribution to larger volumes as evidenced by an increasing integral mean and variance are indicative of longer residence *time paths possibly through more circuitous routes in* the rock. The results of the RTD studies have been incorporated into a general flow model, which is discussed later in detail. Several general comments can be made: (1) The fracture flow system grew considerably in size during the 75-day test, the integrated mean fracture system volume <V> increased to 56,400 ℓ (14,900 gal), up from 37,500 ℓ (9900 gal) on March 1, and the median volume became larger, 48,500 ℓ (12,800 gal) vs 28,800 ℓ (7600 gal). (2) Development of additional flow paths, was evident because of different arrivals of dye with smaller and larger residence times (or volumes), increasing the spread of the distribution. (3) The apparent degree of mixing or dispersion is virtually unchanged between the March 1 *and April 7 experiments as shown by the similar shapes* of the phase I-2, I-3 and I-4 curves on the normalized coordinates of Figs. 4-9 and the similar inverse Peclet numbers resulting from homogeneous, single porous zone fits to the data: Pe^{-1}=0.942 (March 1, 1978), 0.944 (March 23, 1978) and 1.120 (April 7, 1978). (4) The increase in apparent Pe^{-1} observed between the phase I-1 and subsequent tests (I-2, I-3, I-4) cannot be explained by an increase in flow rate from 7.3 to ~14.5 ℓ/s (115 to ~230 gpm). Because we are operating in the freely turbulent region for porous media flow, one would expect a linear dependence of D on u and therefore a constant Pe. Additional flow paths *or a change in the character of flow in existing paths* is a more likely cause of the change in apparent Pe between the early and late tests.

DISCUSSION

Fracture system model

A model of the present fracture system connecting the several wellbores has slowly evolved by the use of conventional logging methods used in the study of oil and gas reservoirs along with measurements obtained from numerous flow tests. The original production hole GT-2 with its accompanying main fracture had only *minimal* connectivity with the EE-1 wellbore-fracture system. The results from numerous flow tests indicated that the main fractures from each wellbore were generally vertical and parallel to each other with a spacing of ~20 m (65 ft). After several attempts to reduce the impedance between these two systems which included extended pressurization, additional fracturing and chemical leaching it was decided to redirect the lower portion of the GT-2 borehole through the *main EE-1 fracture originating at a depth of ~2760 m* (9055 ft)[1]. To do this the GT-2 wellbore was cemented off and the drilling was sidetracked through the wellbore at the top of a cement plug. Figure 9 is an elevation view of the wellbores along with estimated *fracture positions. The fractures are shown as normal* to the figure running in a NW-SE direction. GT-2A the first sidetracked path out of GT-2 is shown as passing over the main EE-1 fracture. During the redrilling of the GT-2 wellbore the EE-1 system was kept pressurized to ~7 MPa (1000 psi) to allow detection of any intercepted fractures. Several pressure changes were noted during the drilling phases apparently when the boreholes intercepted the EE-1 fracture system. Upon completion of GT-2A, the new system was flow tested for system impedance. Although it was significantly lower than the original system it still was not low enough for a major heat extraction test and therefore a second redrilling was started. GT-2B was directed below GT-2A again with EE-1 pressurized. At a depth of 2665 m (8744 ft) a major interception of the EE-1 system was made. After a further short drilling effort which resulted in a second major connection at 2705 m (8870 ft), the new hole was logged and then cased at 2580 m (8465 ft). This new system was tested with a series of short flow experiments which culminated in the major heat extraction experiments.[4] In an attempt to model this complex system, the numerous wellbore logs were examined along with the extensive surveys of the 3-dimensional geometry of the four wellbores passing through the heat extraction zone.[5] The contact between the gneiss and an intruded biotite *granodiorite body[23] shown in Fig. 9 was determined by* well-defined changes in the potassium concentration *as measured by spectral gamma logs for three of the* wellbores. Figure 10 shows a borehole televiewer log run in the original GT-2 borehole by S. Keys of the

United States Geological Survey. The set of inclined fractures detected by this log are roughly parallel with the contact, and their origins may arise from stresses accompanying the intrusion of the granodiorite. The entrace points for fluid in the injection and production wellbores were well defined by the tracer method, temperature and velocity changes in the fluid. Substantial agreement was noted between the locations of these zones and anomalies in caliper, cement bond, and spectral gamma logs. Their grouping at flow points suggests that they mark the intersection of a series of inclined cross fractures with the wellbores. These fractures then provide a degree of lateral communication. Their general inclination and orientation is also parallel with the contact and suggests their origin in the set of natural fractures detected by the televiewer.

Examination of the geometry of the system shows that this set of fractures cannot be the main flow path between the wellbores. A nearly vertical fracture starting from the major flow exit in EE-1 at ~2760 m (9065 ft) which intercepts the set of inclined fractures provides the simplest modeling of both flow measurements and heat transfer data[4]. The sequential arrival of the Br^{82} tracer at the several openings in GT-2B supports such a model.

Aki[1] *has examined acoustic signals arising from* pressurization of this system and deduced their source mechanism. Assuming a vertical principal stress, dip-slip faulting striking NW-SE is his preferred mechanism. Pressurization of the fracture set shown in Fig. 10 could provide events with these characteristics

Dispersional flow modeling

Results of the single zone one-dimensional fit for the phase I-3 dye study are shown in Fig. 11A. In this case, both the flow and volume fractions were set to unity ($\xi_i=\psi_i=1$) and the Peclet number was adjusted to minimize the objective function given in Eq. (4). Although agreement is reasonable, the assumptions concerning the use of a single zone model are questionable. Based on the discussion which led to the fracture model of Fig. 9, flow into and out of the EE-1/GT-2B system is unlikely to be linearly distributed and unidirectional. There are in fact multiple injection and production zones. Furthermore, the apparent level of dispersion is too high, $Pe \gtrsim 1$, for flow in a simple propped fracture. Consequently, we *tried a more realistic approach by attempting to* account for multiple entry and exit points using the multizone model with one-dimensional flow in each zone (Eq. (5)). Figure 11B shows the fit if the flow and volume fractions are fixed and only the Peclet number is varied. Spinner survey results were used to *set the flow fractions while volume fractions were* approximated by the ratio R_i^2/R^2 where R_i=separation distance between the main injection point at 2760 m (9050 ft) and production zone i in GT-2B and R is the effective radius of the main fracture determined by heat transfer modeling[3]. This would be appropriate for constant aperture fractures that behave independently. The theoretical results of Fig. 11B do not match the data any better than they do in the simpler case of Fig. 11A. A third case shown in Fig. 11C allowed both ψ_i and Pe_i to vary and introduced a fifth flow path (∞) which approximated an assumed exponential tail of the C_E-θ curve by a plug flow delay volume followed by an infinitely backmixed region. For this particular set of data it was difficult to observe the tail because the total system volume of ~160,000 ℓ (40,000 gal) was exceeded during recirculation resulting in an overlap of the initial dye pulse. Both smaller ψ_i's and Pe_i's result, suggesting that less dispersion is occurring in smaller volumetric regions between EE-1 and GT-2B. The secondary flow path, approximately 4 to 5% of the total, depicted by the ∞ curve of Fig. 11C also provides a mechanism to explain the geochemical and borehole temperature changes observed during the 75-day test[4]. Small high temperature (~185°C) flows were observed in several zones of GT-2B even after considerable thermal drawdown had occurred[3]. *We believe these secondary flows provide a source of concentrated* silica corresponding to an achieved steady state concentration of 220 ppm which is in agreement with the quartz-controlled saturation value at 185°C.

A two-dimensional type curve match is shown in Fig. 12 with only the formation dependent Peclet number (Pe^*) variations shown. Satisfactory agreement occurs when $Pe^* \gtrsim 1.0$ with a match point at t=3940 s and θ=4.4. Assuming that the area of the system is confined to the value obtained from heat transfer modeling ($2a \doteq 100$ ft) the product of fracture aperture and porosity (hs) is about 2 cm.

Simplifications are inherent to all the models with effects such as flow channeling, stagnation in pockets, fracture aperture variations neglected. However, the incorporation of these effects will introduce more parameters which are of course adjustable empirically and consequently the "theoretical" fit will improve. For the models considered in this paper additional degrees of freedom were obtained by going from the single zone one-dimensional system to either *the multizone model with up to 3 M parameters in* Pe_i, ξ_i, and ψ_i for M zones or the two-dimensional system with D^*, a_x/a, and k adjustable.

CONCLUSIONS

1. Borehole tracer techniques using T^{131} and Br^{82} have been successfully used at temperatures up to 200°C and depths to 3 km (10,000 ft) to quantitatively characterize flow at injection and production points in hydraulically fractured regions in granite.

2. Residence time distribution methods using sodium fluorescein tracers characterized fracture volumes and levels of dispersed mixing.

3. Combined use of geophysical, geometric, and flow data and one- and two-dimensional dispersion analyses provided an interpretive method for developing plausible reservoir models for hydraulically fractured hot dry rock systems. Because of the complex geometric relationships (fracture roughness, primary and secondary flow paths through propped joints, dead end *pore volume and other stagnation regions) which* control the dispersion and mixing parameters a unique model was not determined.

ACKNOWLEDGEMENTS

The authors would like to thank C. O. Grigsby, J. Abbott, R. Spence, J. Hill, J. Skalski and R. Hendron for their assistance in the experimental phases of these tests. J. Archuleta, C. Fink and J. Kurtenbach were responsible for the design and construction of the Br^{82} tool. The assistance provided by Doris Elsner in the preparation of the manuscript is greatly appreciated. The support of the Division of Geothermal Energy of the U. S. Department of Energy is also gratefully acknowledged.

NOMENCLATURE

a = vertical half well spacing between injection and production zones - m(ft)
C_i = measured tracer concentration at time t_i-ppm
C_θ = dimensionless tracer concentration
C_θ^* = normalized tracer concentration
D = dispersion coefficient-m^2/s (ft^2/s)
D^* = formation dependent dispersion coefficient
h = thickness of zone or fracture aperture-m(ft)
$k = \alpha_x/\alpha_y$ = ratio of transverse (y) to longitudinal (x) dispersional velocity components
L = flow length for one-dimensional model-m(ft)
$Pe = \frac{uL}{D^*}$ = one-dimensional, dispersional Peclet number
Pe^* = two-dimensional, dispersional Peclet number
q = flow rate - m^3/s (gpm)
q_ℓ = flow rate per unit thickness (h) - m^2/s (ft^2/s)
R = effective radius of fracture based on heat transfer data = 100 m (300 ft)
t = time - s
u = interstitial linear flow velocity - m/s (ft/s)
V = fracture system volume - ℓ or m^3(gal)
$[V]$ = median fracture system volume - ℓ or m^3(gal)
$\langle V \rangle$ = integral mean fracture system volume - ℓ or m^3(gal)
$|V|$ = trimmed mean fracture system volume - ℓ or m^3(gal)
V^* = truncation volume ℓ or m^3(gal)
α_x = x-direction velocity component of the dispersion coefficient - m(ft)
α_y = y-direction velocity component of the dispersion coefficient - m(ft)
ϕ = porosity
ϕ_U^* = dimensionless x-direction velocity profile function
ϕ_V^* = dimensionless y-direction velocity profile function
σ_θ^2 = C_θ-residence time distribution variance
$\bar{\tau}$ = $\langle V \rangle / q$ = integral mean residence time - s
θ = dimensionless time or volume
ξ_j = q_j/Q = flow fraction for production zone j
ψ_j = V_j/V = volume fraction for production zone j

REFERENCES

1. Hot Dry Rock Geothermal Energy Development Project, *Annual Report Fiscal Year 1977*, Los Alamos Scientific Laboratory report LA-7109-PR, Los Alamos, NM (Feb. 1978).

2. Brown, M. C., Duffield, R. G., Sicilianu, C. L. B., and Smith, M. C. (eds.), "Hot Dry Rock Geothermal Energy Development Program," Los Alamos Scientific Laboratory report LA-7807-HDR, Los Alamos, NM (April 1979).

3. Murphy, H. and Tester, J. W., "Heat Production from a Hot Dry Rock Geothermal Reservoir Formed by Hydraulic Fracturing -- A Comparison of Field and Theoretical Results," paper SPE-8265 presented at 54th SPE-AIME Annual Technical Conference and Exposition, Las Vegas, NV (Sept. 23-26, 1979).

4. Tester, J. W. and Albright, J. N. (eds.), "Hot Dry Rock Energy Extraction Field Test: 75 Days of Operation of a Prototype Reservoir at Fenton Hill," Los Alamos Scientific Laboratory report LA-7771-MS, Los Alamos, NM (April 1979).

5. Potter, R. M., "Hydraulic Fracture Initiation Sites in Open Boreholes Identified by Geophysical Logs," proceedings of 3rd Annual Workshop on Geothermal Reservoir Engineering, Stanford University Stanford, CA (Dec. 14-16, 1977).

6. Wagner, O. R., "The Use of Tracers in Diagnosing Interwell Reservoir Heterogeneities -- Field Results," J. of Petroleum Technology, p. 1410-1416 (1977).

7. Wagner, O. R., Baker, L. E., and Scott, G. R., "The Design and Implementation of Multiple Tracer Program for Multifluid, Multiwell Injection Projects," paper SPE 5125 presented at SPE-AIME 49th Annual Fall Meeting, Houston (Oct. 6-9, 1974).

8. Ogata, A., "Theory of Dispersion in a Granular Medium," Geological Survey Professional Paper 411-I, U.S. Govt. Printing Office, Washington, D.C. (1970).

9. Brigham, W. E. and Smith, Jr., D. H., "Prediction of Tracer Behavior in Five-Spot Flow," paper SPE 1130 presented at SPE-AIME 40th Annual Fall Meeting, Denver (Oct. 3-6, 1965).

10. Grove, D. B. and Beetan, W. A., "Porosity and *Dispersion Constant Calculations for a Fractured* Carbonate Aquifer Using the Two Well Tracer Method," Water Resources Research 7 (1), pp. 128-134 (1971).

11. Webster, D. S., Procter, J. F., and Marine, I. W., "Two-Well Tracer Test in Fractured Crystalline Rock," in General Ground-Water Techniques Geological Survey Water-Supply paper 1544-I, Washington, D. C. (1970).

12. Levenspiel, O. and Smith, W. K., "Notes on the Diffusion Type Model for Longitudinal Mixing of Fluids in Flow," Chem. Eng. Science 6, pp. 227-233 (1957).

13. Brenner, H., "The Diffusion Model of Longitudinal Mixing in Beds of Finite Length-Numerical Values," Chem. Eng. Science 17, pp. 229-243 (1962).

14. Taylor, G. I., "Dispersion of Soluble Matter in Solvent Flowing Slowly Through a Tube," Proc. Roy. Soc., London A219, pp. 186-203 (1953).

15. Taylor, G. I., "Dispersion of Matter in Turbulent Flow Through a Pipe," Proc. Roy. Soc., London A223, pp. 446-468 (1954).

16. Shamir, U. Y. and Harleman, D. R. F., "Numerical Solutions for Dispersion in Porous Mediums," Water Resources Research 3 (2), pp. 557-581 (1967).

17. Deans, H. A., "A Mathematical Model for Dispersion in the Direction of Flow in Porous Media," Soc. Petro. Eng. J. 3 (1), pp. 49-52 (March 1963).

18. Coats, K. H. and Smith, B. D., "Dead-End Pore Volume and Dispersion in Porous Media," Soc. Petro. Eng. J. 4 (1), pp. 73-84 (March 1964).

19. Baker, L. E., "Effects of Dispersion and Dead-End Pore Volume in Miscible Flooding," Soc. Petro. Eng. J. 17, pp. 219-227 (June 1977).

20. Donaldson, E. C., Kendall, R. F., and Manning, F. S., "Dispersion and Tortuosity in Sandstones," paper SPE 6190 presented at SPE-AIME 51st Annual Fall Technical Conference and Exhibition, New Orleans (Oct. 3-6, 1976).

21. Maranville, M. B., Kessler, D. P., and Greenkorn, R. A., "Dispersion in Layered Porous Media," AIChE J. 23 (6), pp. 786-794 (1977).

22. Levich, V. G., Markin, V. S., and Chismadzhev, Y. A., "On Hydrodynamic Mixing in a Model of a Porous Medium with Stagnant Zones," Chem. Eng. Science 22, pp. 1357-1367 (1967).

23. Laughlin, A. W., "The Geothermal System of the Jemez Mountains, New Mexico and Its Exploration," a chapter to appear in The Jemez Mountains, New Mexico, edited by J. P. Muffler [to be published].

24. Roache, P. J., Computational Fluid Dynamics, Hermosa Publishers, Albuquerque, NM, p. 64 (1972).

APPENDIX A - TWO-DIMENSIONAL DISPERSION AND TYPE CURVES

For the two-dimensional, steady flow case, equation (1) is rewritten as:

$$\frac{\partial}{\partial x}\left(D_x \frac{\partial C}{\partial x}\right) + \frac{\partial}{\partial y}\left(D_y \frac{\partial C}{\partial y}\right) - u\frac{\partial C}{\partial x} - v\frac{\partial C}{\partial y} = \frac{\partial C}{\partial t} \quad \ldots\ldots (A\text{-}1)$$

where D_x and D_y are given by equation (7). The initial condition is:

$$C = C(x,y,t=0) = 0 \text{ at all } x \text{ and } y$$

and with the injector located at $x = -a$, $y = 0$ and the producer at $x = +a$, $y = 0$, the boundary conditions are:

$$C(-a,0,t) = C^o \text{ at the injection well } t>0$$

$$C(\pm\infty,\pm\infty,t) = 0 \qquad t>0$$

Equation (A-1) can be expressed in dimensionless form as

$$\frac{\partial}{\partial X}\left[\frac{\alpha_x}{a}\phi_u^* + \frac{1}{Pe^*}\right]\frac{\partial C_\theta}{\partial X} + \frac{\partial}{\partial Y}\left[k\frac{\alpha_x}{a}\phi_v^* + \frac{1}{Pe^*}\right]\frac{\partial C_\theta}{\partial Y} - \phi_u^*\frac{\partial C_\theta}{\partial Y} - \phi_v^*\frac{\partial C_\theta}{\partial Y} = \frac{\partial C_\theta}{\partial \theta} \quad \ldots\ldots (A\text{-}2)$$

using equation (7) and the following definitions

$$X = x/a \qquad Pe^* = \frac{\dot{q}}{h\phi D^o} \qquad k = \frac{\alpha_y}{\alpha_x}$$

$$Y = y/a \qquad \theta = \frac{\dot{q}t}{h\phi a^2}$$

$$C_\theta = C/C^o$$

ϕ_u^* and ϕ_v^* are the dimensionless velocity functions from the steady state flow solution:

$$\phi_u^* = \frac{va\phi h}{\dot{q}} = \frac{1}{2\pi}\left[\frac{X+1}{(X+1)^2+Y^2} - \frac{X-1}{(X-1)^2+Y^2}\right] \quad \ldots\ldots (A\text{-}3)$$

$$\phi_v^* = \frac{va\phi h}{\dot{q}} = \frac{1}{2\pi}\left[\frac{Y}{(X+1)^2+Y^2} - \frac{Y}{(X-1)^2+Y^2}\right] \quad \ldots\ldots (A\text{-}4)$$

Equation (A-2) was solved numerically using a modified finite difference approach with an upwind differencing technique suggested by Roache[24]. An alternating direction implicit algorithm resulted in stable and convergent results. The lower set of cells were centered on the x-axis. Because of symmetry along this no flux boundary, the problem was solved only in the positive y quadrants. Horizontally, a uniform mesh was used between wells and for 5 additional cells on either side. Vertically, the same uniform mesh size was extended by an equivalent number of cells as contained between wells. Horizontally and vertically beyond these boundaries, an expanding mesh size (e.g. $\Delta X_i = 1.5\,\Delta X_{i-1}$). For small values of $Pe<5$, smaller time steps $\Delta\theta<0.005$ were required for convergence. Similar requirements were necessary if $\alpha_x/a \geq 0.5$ with $k=0.1$.

Semi-logarithmic type curves were constructed to show the effects of Pe^*, α_x/a, and k. Four of these are shown in Figs. A-1 - A-4.

TABLE 1

RESIDENCE-TIME DISTRIBUTION RESULTS

EXPERIMENT	Q 10^6 gal	$\bar{q}$ gpm[b]	dye recovery (%)	$\langle V \rangle$ gal[c]	$[V]$ gal	$\lvert V \rvert$ at 90% gal	σ_θ^2	σ_θ^2 (90%)	Pe^{-1}[d]
Phase 1-1 (2/9/78)	2.1	115	69	9089	6753	7728	0.65	0.44	0.591
Phase 1-2 (3/1/78)	6.9	208	65	9899	7644	8160	0.62	0.43	0.942
Phase 1-3 (3/23/78)	15.1	220	71[a]	14446	11904	12218	0.51	0.42	0.944
Phase 1-4 (4/7/78)	20.0	240	>65[a]	14855	12786	12998	0.47	0.39	1.120

[a] Estimated from extrapolation of the RTD tail shown in Fig. 7; actual recovery to 40,000 gal was 63% for 1-3 and 57% for 1-4.

[b] 1 gpm = 6.31×10^{-2} liters/s (ℓ/s).

[c] 1 gal = 3.785 liters.

[d] Pe^{-1} = D°/uL = inverse Peclet number for one-dimensional, single zone fit.

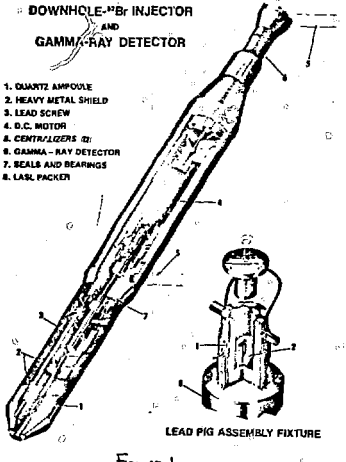

Figure 1

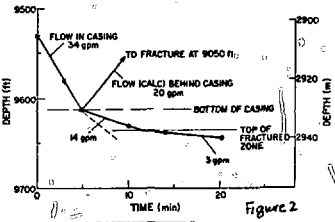

Figure 2

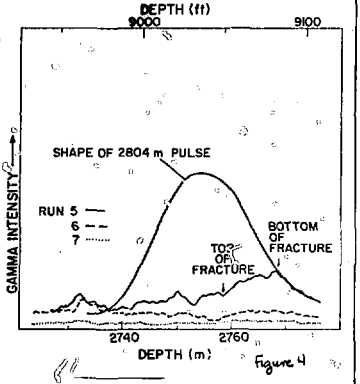

Figure 4

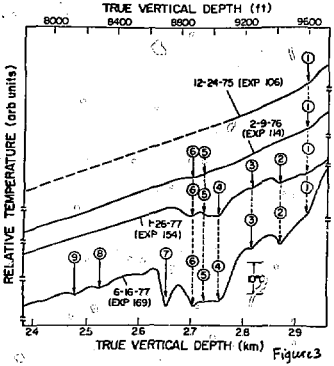

Figure 3

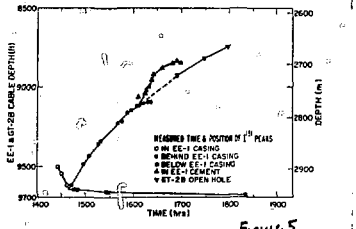

Figure 5

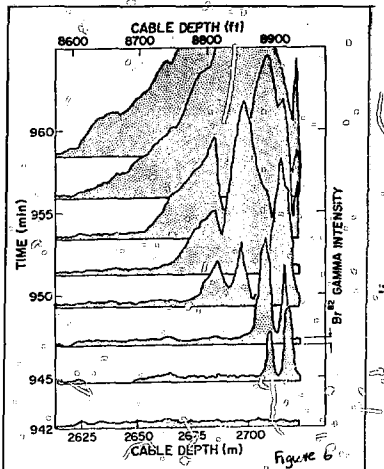

Figure 6

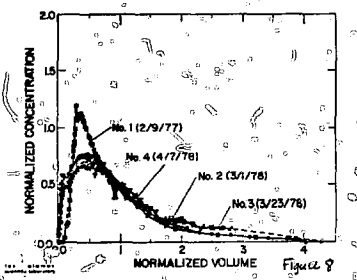

Figure 8

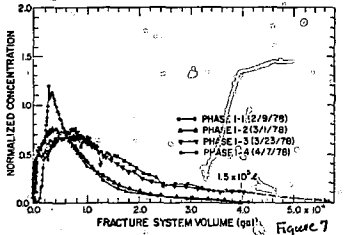

Figure 7

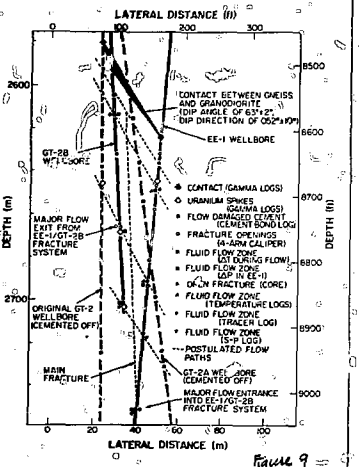

Figure 9

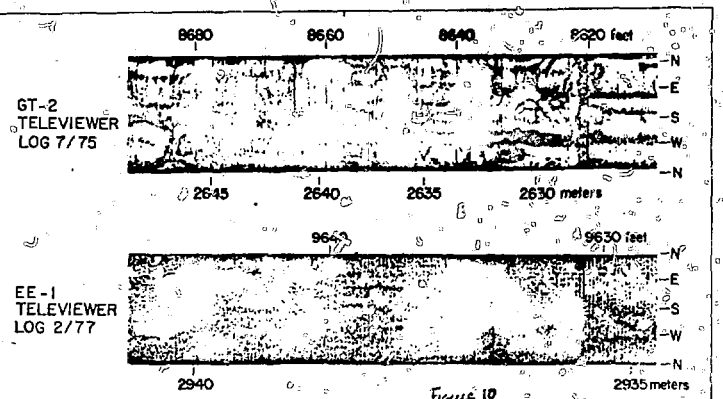

Figure 10

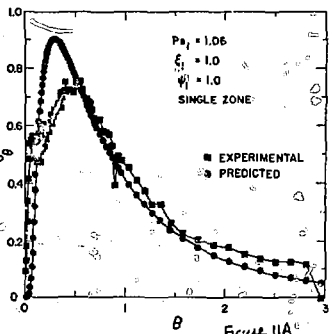

Figure 11A

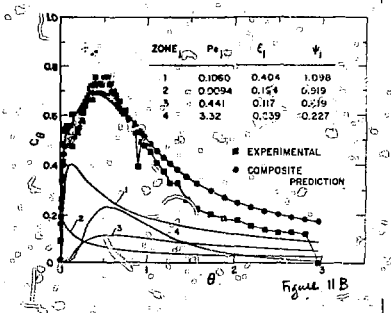

Figure 11B

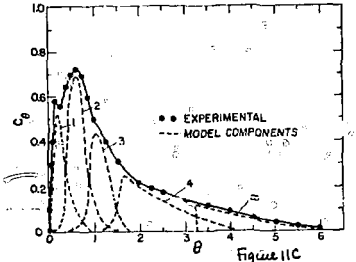

Figure 11C

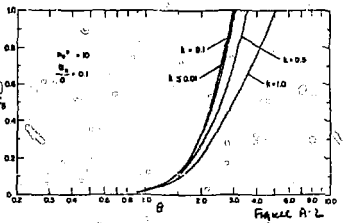

Figure A-2

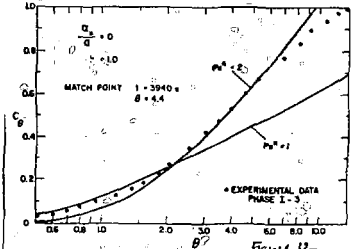

Figure 12

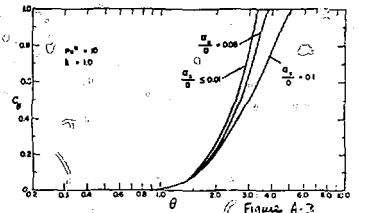

Figure A-3

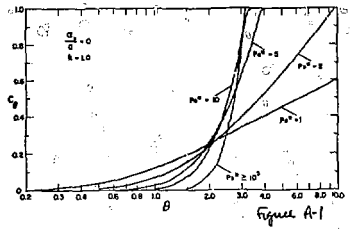

Figure A-1

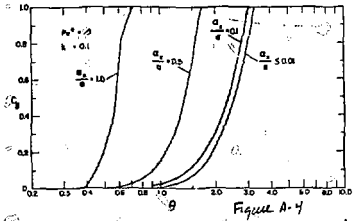

Figure A-4

TABLE 1

RESIDENCE-TIME DISTRIBUTION RESULTS

EXPERIMENT	Q 10^6 gal	$\bar{q}$ gpm[b]	dye recovery (%)	$\langle V \rangle$ gal[c]	$[V]$ gal	$\lvert V \rvert$ at 90% gal	σ_θ^2	σ_θ^2 (90%)	Pe^{-1}[d]
Phase I-1 (2/9/78)	2.1	115	69	9089	6753	7728	0.65	0.44	0.591
Phase I-2 (3/1/78)	6.9	208	65	9899	7644	8160	0.62	0.43	0.942
Phase I-3 (3/23/78)	15.1	220	71[a]	14446	11904	12218	0.51	0.42	0.944
Phase I-4 (4/7/78)	20.0	240	> 65[a]	14855	12786	12998	0.47	0.39	1.120

[a]Estimated from extrapolation of the RTD tail shown in Fig. 7; actual recovery to 40,000 gal was 63% for I-3 and 57% for I-4.

[b]1 gpm = 6.31×10^{-2} liters/s (ℓ/s).

[c]1 gal = 3.785 liters.

[d]$Pe^{-1} = D/uL$ = inverse Peclet number for one-dimensional, single zone fit.

LIST OF FIGURES

APPENDIX

LIST OF FIGURES (Continued)